MOMENTUM DISTRIBUTION AND CHARGE RATIO OF μ-MESONS AT ZENITH ANGLES IN THE EAST–WEST PLANE

By J. R. Moroney* and J. K. Parry*

[*Manuscript received June* 2, 1954]

Summary

The momentum distribution and charge ratio of the penetrating component of the cosmic radiation at sea-level have been determined over the momentum range 0·24–58 BeV/c at a geomagnetic latitude of 47 °S. The measurements were performed in the vertical direction and at zenith angles of 30° and 60° in the eastern and western azimuths.

An attempt has been made to calculate the sea-level spectra at these zenith angles on the basis of a simplified continuous production process. A comparison with the measurements indicates that, although the calculations describe the general behaviour, the quantitative agreement is unsatisfactory. The charge ratios measured at zenith angles in the western azimuth increase, and those in the eastern azimuth decrease, as the momentum decreases. This is explained as a secondary effect due to curvature of the meson trajectories in the magnetic field of the Earth. Information has been obtained on the dependence of the exponent n on the momentum, where n is defined by the intensity-zenith angle relation, $I_\theta = I_0 \cos^n \theta$. From the value 3·3 at 0·3 BeV/c, n approaches zero at high momentum. The radiation is approximately isotropic above 20 BeV/c.

I. Introduction

In recent years a number of careful studies (Wilson 1946 ; Caro, Parry, and Rathgeber 1951 ; Owen and Wilson 1951 ; Beretta *et al.* 1953 ; and others) have been made of the momentum distribution and charge ratio of the penetrating component of cosmic radiation incident in the vertical direction. However, no comparable information is available on the radiation observed at inclinations to the vertical.

In an endeavour to extend the experimental knowledge in this region a measurement has been made of the momentum distribution and charge ratio of the penetrating component at angles of 30° and 60° in the east-west plane. The experiment was performed at sea-level at a geomagnetic latitude (Melbourne) of 47 °S.

II. Method

The spectrometer used to determine the momentum and sign of single charged particles has been described previously (Caro, Parry, and Rathgeber 1951). The particles are deflected in the air gap of an electromagnet and the extent of the deflexion is measured by trays of Geiger counters. Additional counters under 10 cm of lead identify the penetrating component. It should be emphasized that this technique discriminates against penetrating particles

* Physics Department, University of Melbourne.

accompanied by shower particles; an unambiguous interpretation is possible only for single particles.

In order to cover the maximum momentum range, from the momentum cut-off imposed by the 10 cm of lead to the resolving limit of the instrument, the measurements are conducted at two values of the magnetic field. The momentum ranges covered at 1900 and 13,500 G are respectively 0·24–10 BeV/c and 1·3–70 BeV/c. At low momenta the measured spectrum is subject to instrumental distortion due to a magnetic cut-off effect. The results are corrected for this effect as described in the previous paper.

III. Results

The results have been obtained in 10 separate measurements; those taken at 13,500 G in the vertical direction have been published previously (Caro, Parry, and Rathgeber 1951) but are included here for completeness. Table 1 gives the number of particles analysed in each measurement. The results of each determination were analysed using the methods discussed in the previous

Table 1

DETAILS OF THE TOTAL NUMBER OF PARTICLES RECORDED IN EACH MEASUREMENT AND THE ABSOLUTE INTENSITY AT EACH ZENITH ANGLE

Measurement	Number of Particles Recorded		Corrected Intensity (sterad^{-1} cm^{-2} sec^{-1})
	1900 G	13,500 G	
Vertical	3971	2127	$(8{\cdot}20 \pm 0{\cdot}26) \times 10^{-3}$
30 °E.	1304	2797	$(6{\cdot}22 \pm 0{\cdot}27) \times 10^{-3}$
30 °W.	1523	1410	$(6{\cdot}12 \pm 0{\cdot}24) \times 10^{-3}$
60 °E.	1230	1234	$(1{\cdot}90 \pm 0{\cdot}09) \times 10^{-3}$
60 °W.	2168	1385	$(1{\cdot}83 \pm 0{\cdot}09) \times 10^{-3}$

paper, corrections for magnetic cut-off were applied, and the differential momentum spectra constructed. The particles were grouped into momentum intervals chosen to give adequate momentum resolution with good statistics. The weighted mean momentum of each interval was used in plotting the results. Each 13,500 G determination of the momentum spectrum was normalized to its 1900 G counterpart by equating the number of particles recorded with momentum greater than 1·3 BeV/c.

Since the instrument was inoperative for 20 sec while each record was produced it has been necessary to correct the counting rate for this dead time. The absolute intensity at each zenith angle was computed from the known geometry of the counter telescope. These intensities are shown in Table 1.

The differential momentum spectra of the positive particles, the negative particles, and the total penetrating component normalized to the correct absolute intensities are plotted in Figures 1 (*a*)–(*e*) for each zenith angle. The smooth curves are drawn through by eye and are intended to represent the best fit to the results.

IV. Discussion

The penetrating component at sea-level is known to consist predominantly of μ-mesons. An estimate based on the work of Mylroi and Wilson (1951) indicates that less than 0·5 per cent. of the penetrating particles recorded in the

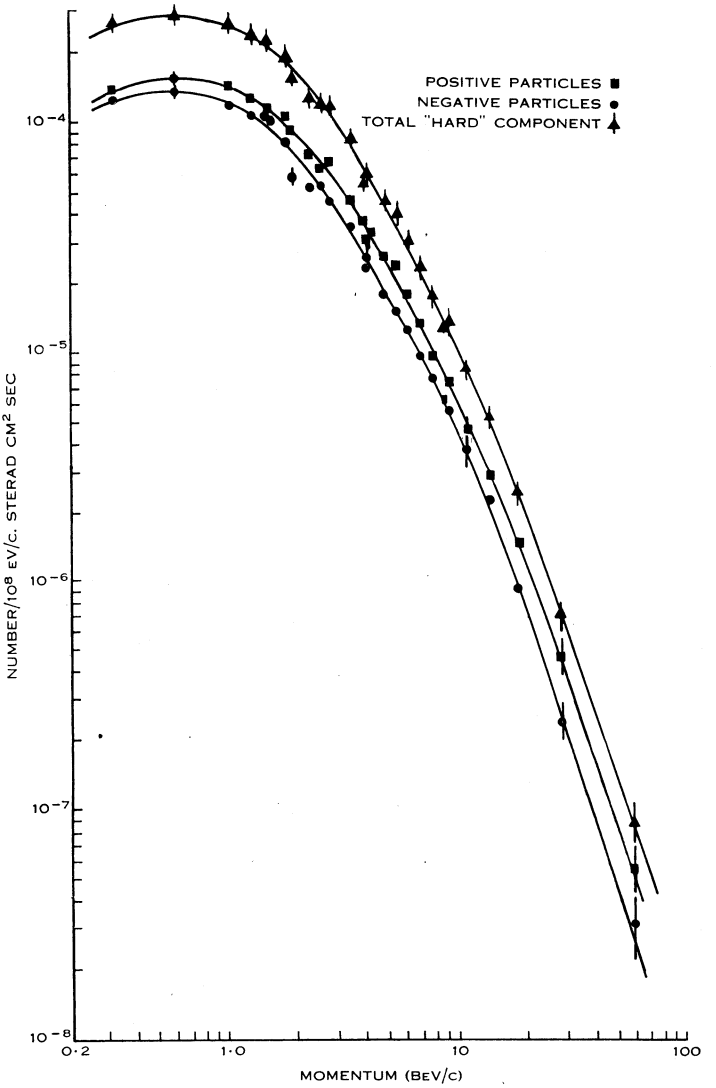

Fig. 1 (*a*).—Vertical differential momentum spectra.

vertical direction are protons. Other possible contributions are from high energy single electrons and π-mesons. Since only events in which a single counter under the lead is discharged are accepted for analysis, the contribution from high energy electrons may be neglected. Little is known of the intensity of high energy single π-mesons at sea-level but there is no evidence to suggest that this

is appreciable. Since no calculation in the following section is accurate to better than 5 per cent. it is felt that no significant error is made if, for the purpose of comparison with calculations, the penetrating component in all measurements is identified with the μ-meson component.

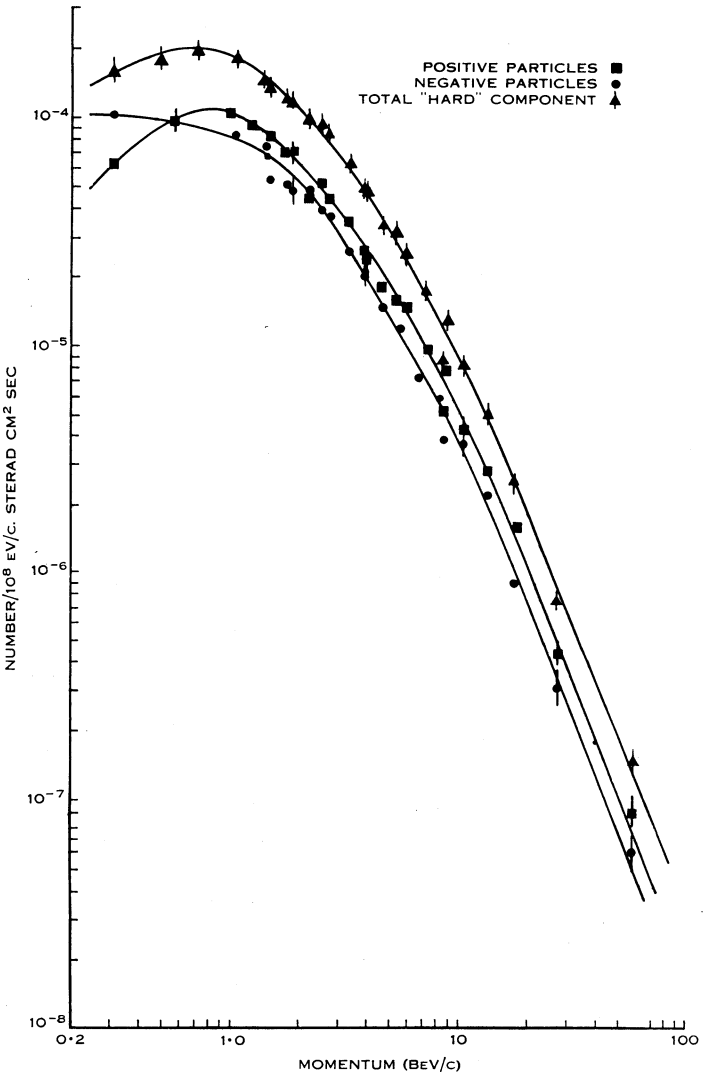

Fig. 1 (*b*).—30 °E. differential momentum spectra.

(*a*) *The Total Spectra at Zenith Angles of 0°, 30°, and 60°*

(i) *Introduction.*—The smooth curves representing the differential spectra of the μ-meson component in the five directions are shown together in Figure 2. It is apparent that the main effect observed is the increasing attenuation of the low momentum intensity with zenith angle. The differences between the spectra

measured in the eastern and western azimuths for a given zenith angle, and between all spectra above 20 BeV/c, are not considered significant when the statistical accuracy of the points is taken into account. Although at the latitude of this experiment a small east-west asymmetry is known to exist, 0·01 at 30°

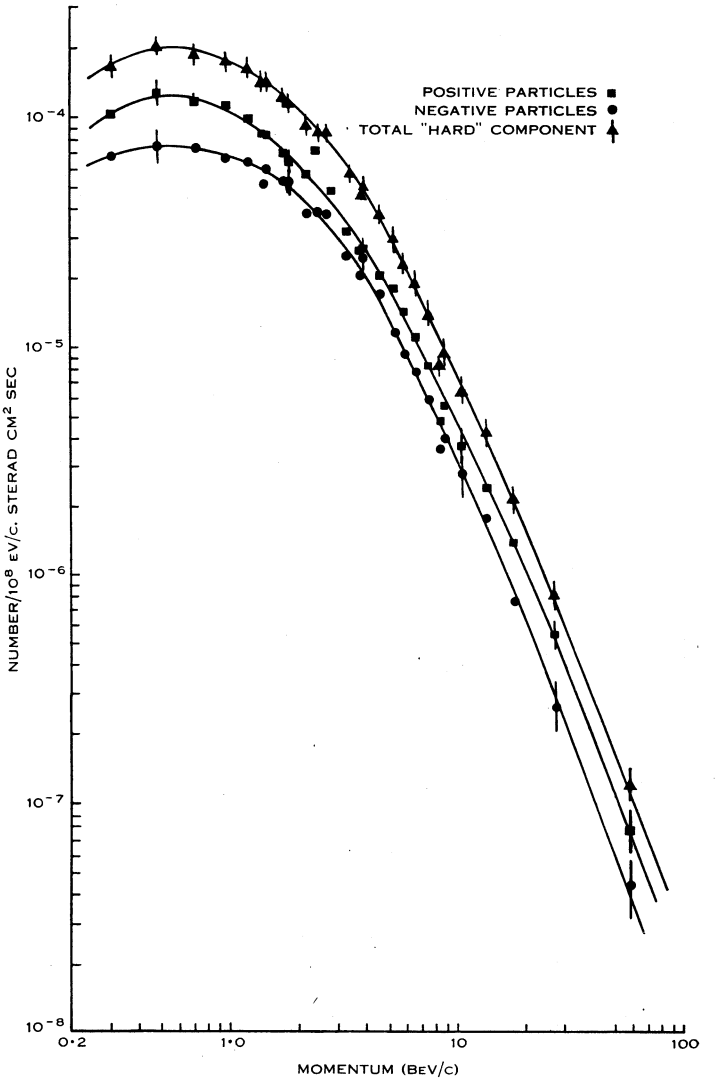

Fig. 1 (*c*).—30 °W. differential momentum spectra.

and 0·03 at 60° (Burbury and Fenton 1952), the accuracy of the absolute rate determination was insufficient for this to be detected.

A series of calculations has been made to determine whether the dependence of the total spectra on zenith angle can be explained solely in terms of the differing decay and momentum loss suffered by the μ-mesons in their paths through the atmosphere. The primary radiation, from which these particles

arise, is considered to be essentialy isotropic at the top of the atmosphere since the geomagnetic latitude, 47 °S, is at the knee of the latitude effect. In this section no account is taken of charge-sensitive phenomena within the atmosphere so that the μ-mesons are assumed to follow straight paths to sea-level.

The calculation falls into two parts; the tabulation of the survival probabilities and the derivation of a production spectrum which gives a reasonable and consistent description of the observed sea-level spectra.

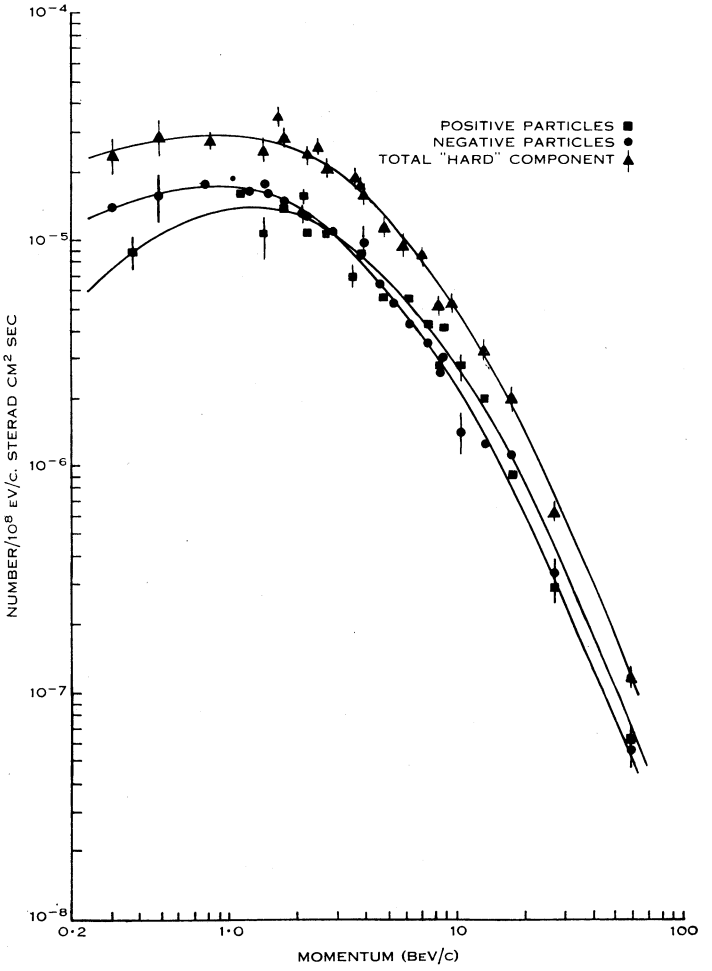

Fig. 1 (*d*).—60 °E. differential momentum spectra.

(ii) *Survival Probabilities.*—Denote by $w(x_0, p_0, \theta)$ the probability that a μ-meson will survive to sea-level and be recorded with momentum p_0, at a zenith angle θ after production at a distance x_0 cm from sea-level, measured along its path. Then

$$w(x_0, p_0, \theta) = \exp\left[-\frac{1}{\tau c}\int_0^{x_0} \frac{\mathrm{d}x}{p(x)}\right],$$

with $p(x)$ representing the momentum in units of μc at the distance x cm along the path. The function $p(x)$ may be evaluated by means of the range-momentum relation and a knowledge of the variation of absorber thickness along the track. A graphical representation of the distance-range relation, $x=f_\theta(R)$, was derived from pressure-altitude data provided by the Melbourne Meteorological Bureau. Here R g cm^{-2} is the absorber thickness traversed to sea-level from x. The

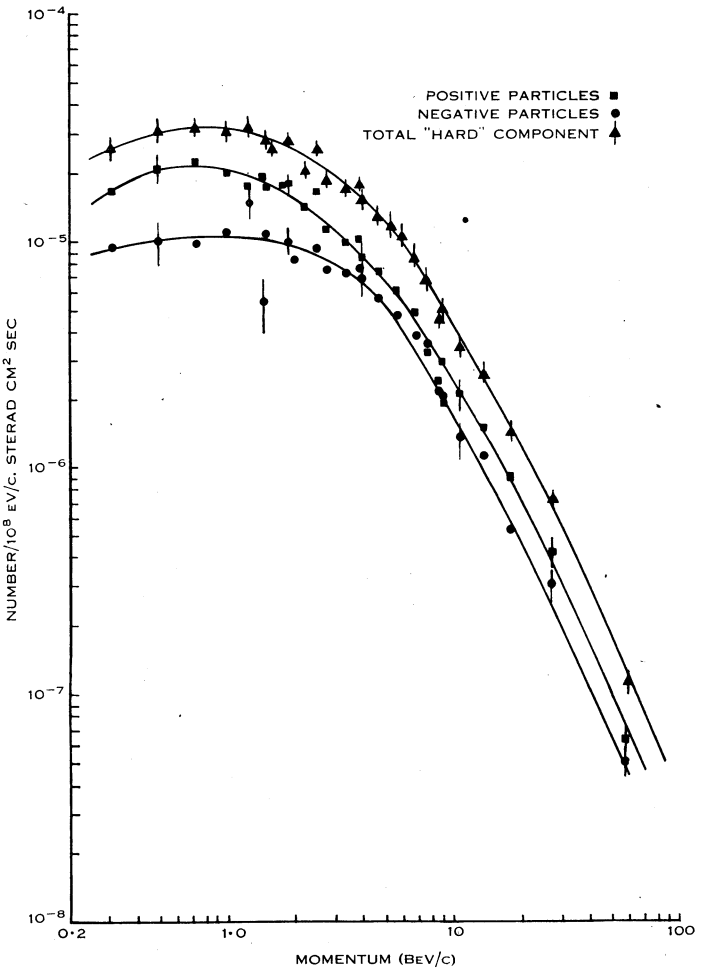

Fig. 1 (*e*).—60 °W. differential momentum spectra.

numerical values of the function $p(f_\theta(R))$ used in the integration were obtained from the tabulated results of a range-momentum calculation (Fenton 1952).

The proper mean life τ and rest mass μ of the μ-meson were taken as $2{\cdot}15\times10^{-6}$ sec and 210 electron masses respectively, and the integral evaluated numerically at the zenith angles 0°, 30°, and 60°. A family of curves was obtained for each angle describing the variation of survival probability with height of production in g cm^{-2}, at eight values of the sea-level momentum p_0.

(iii) *Single Layer Production.*—A reasonable description of the vertical spectrum has been found to be given by a process involving production at a single level near the top of the atmosphere (Euler and Heisenberg 1938 ; Janossy and Wilson 1946). When the decay of the mesons and the loss of momentum by ionization were taken into account, the production spectrum was shown to have the form of an inverse power law. Following the method of Janossy and Wilson (1946), a calculation was performed which indicated that the three sea-level spectra cannot be described simultaneously by a production process of

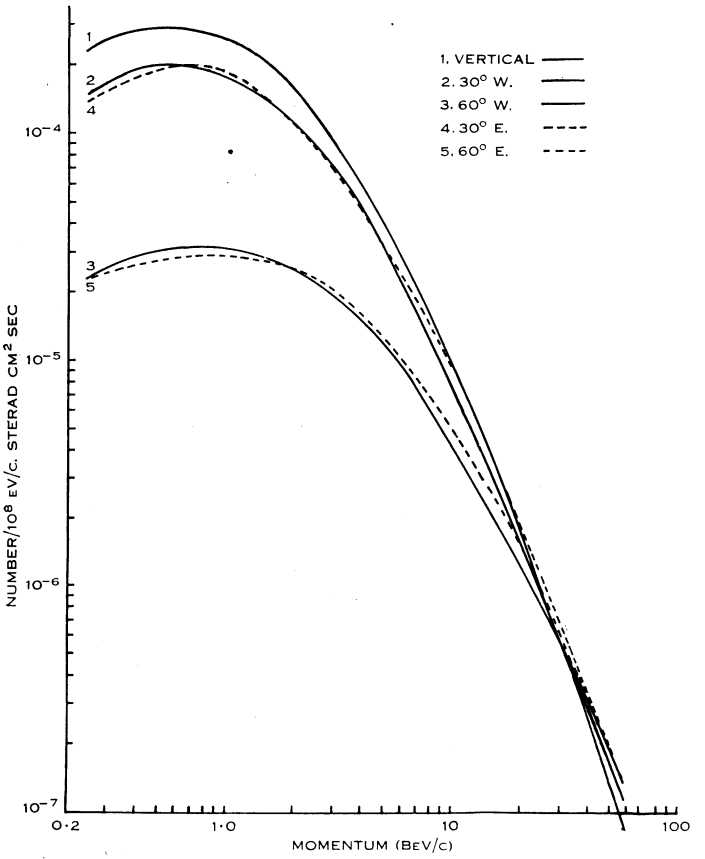

Fig. 2.—Zenith angle variation of the differential momentum spectrum—total hard component.

this nature. Moreover, these calculations showed, in agreement with conclusions reached by Sands (1950), that the mean height of production of μ-mesons reaching sea-level with a particular momentum decreases with decreasing momentum. For an adequate description, some form of extended production must be considered.

(iv) *Extended Production.*—The simplest model of an extended production process has been proposed by Sands (1950) who assumes that the dependences of production on depth and on momentum are separable. It is also assumed

that the production of mesons as a function of depth follows the same law as the absorption of the primary component. This is given by $\exp(-r/125)$ where r g cm^{-2} is the depth from the top of the atmosphere measured along the path. As pointed out by Sands (1950) there is some justification for this separation at small values of r, but at greater atmospheric depths, where a secondary meson producing component may be appreciable, this assumption would break down.

It is known that the momentum dependent part of the production function is given to a good approximation by an inverse power law for momenta above several BeV/c. The behaviour of the function at low momenta may be obtained by fitting the results. The production spectrum obtained in this manner has the form

$$0{\cdot}147(p)^{-3{\cdot}0}.\ \exp(-r/125) \qquad \text{for } p > 17{\cdot}6\ \mu c,$$
$$0{\cdot}147(17{\cdot}6)^{-3{\cdot}0}.\ \exp(-r/125) \qquad \text{for } p \leqslant 17{\cdot}6\ \mu c,$$

where the intensity is in units of number of mesons $(10^8\ \text{eV/c})^{-1}\ \text{cm}^{-2}\ \text{sec}^{-1}$. This spectrum differs from that found by Sands (1950). The spectrum derived by this author was based on observations of the low momentum intensity in the vertical direction at sea-level and at various altitudes. Although his spectrum is undoubtedly more reliable in the low momentum region it fails to give satisfactory agreement with the present results at high momentum.

The sea-level spectra were calculated by integrating the product of the production spectrum and survival probabilities over the atmosphere. These calculated spectra are compared with the measurements in Figure 3. Since only the total μ-meson component is considered it is felt that little error is made by combining the measurements in the eastern and western azimuths. The calculated spectra are normalized to the vertical observations at a momentum of 1·3 BeV/c.

Although the agreement is better than that achieved assuming single layer production it remains unsatisfactory. From Figure 3 it is seen that the vertical and 30° distributions, which were used in deriving the production spectrum, are adequately represented but that the calculated intensity at the 60° zenith angle is approximately 50 per cent. too low over a considerable region. At this angle, meson production as described by the depth dependent function, is already negligible at atmospheric depths such that mesons reaching sea-level are produced with momentum above the cut-off value, 17·6 μc.

A similar discrepancy was observed by Kraushaar (1949) who calculated the relative intensities of slow mesons at these zenith angles using a modified form of Sands' production spectrum. The above calculations have assumed that the mesons preserve the direction of the primary particles, however, it is known that at low momenta an appreciable spread is introduced due to both Coulomb scattering and the meson-producing events. No quantitative information is available on the angular distribution of the emitted mesons as a function of their momentum. However, taking the results of Brown *et al.* (1949) to refer to low momentum mesons, an approximate calculation was made to determine

the effect of this spread on mesons of 0·6 BeV/c at sea-level. The calculation shows that this effect is of the right order to account for the observed discrepancy. At high momentum these considerations are less important and the original assumptions will not be greatly in error.

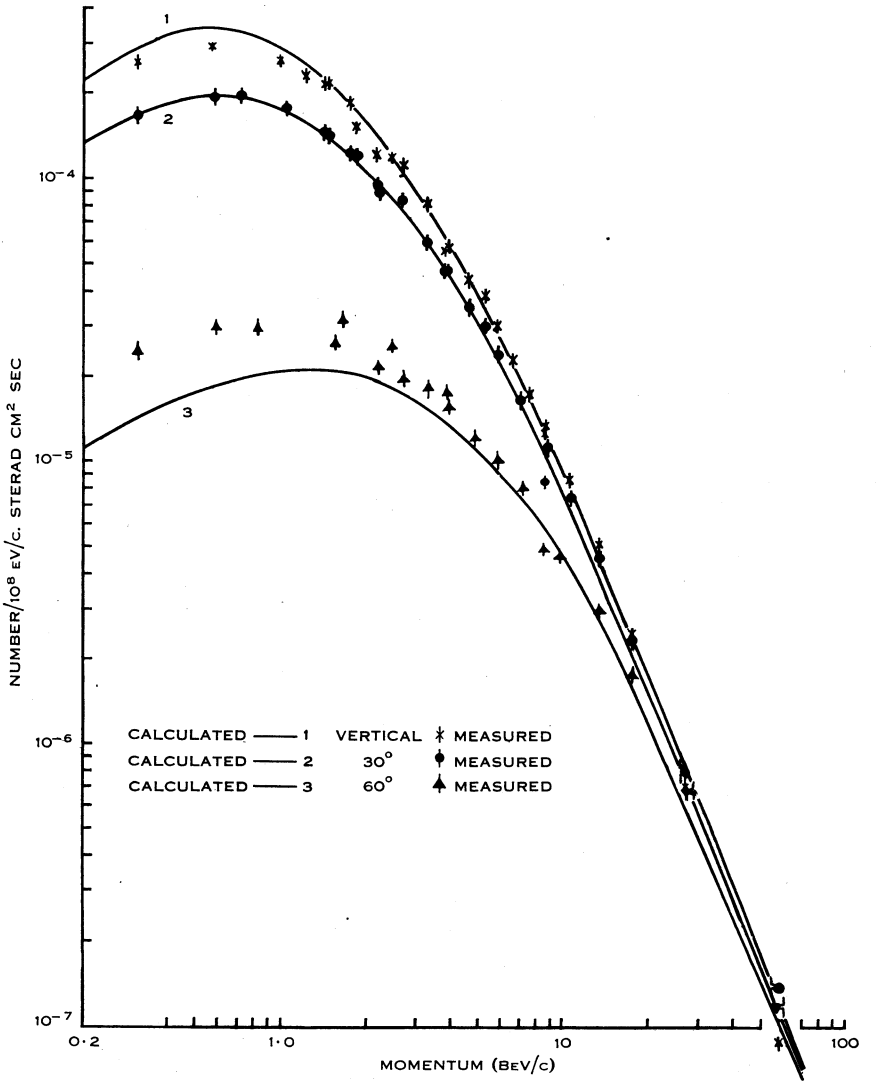

Fig. 3.—Differential momentum spectra.

(b) The Positive and Negative Spectra and the Charge Ratio

It may be seen from Figure 1 (*a*) that the positive and negative spectra obtained in the vertical direction have the same form and an approximately constant intensity ratio over the momentum range investigated. However, at inclinations to the vertical, Figures 1 (*b*)–(*e*), the positive and negative spectra differ in form and vary systematically as a function of zenith angle and

momentum. This effect manifests itself as large variations in the charge ratio (i.e. the ratio of the intensities of the positive and negative particles) and, since the results may be discussed more readily in terms of this quantity, we proceed to examine its behaviour.

The charge ratio in a given momentum interval may be obtained directly from the results. In order to determine the behaviour of this ratio as a function of momentum it is necessary to compromise between good momentum resolution and good statistics. This has been achieved by splitting the 1900 G measurements into three momentum intervals and the 13,500 G measurements into four intervals. The details of the momentum range and mean momentum (weighted by the distribution of particles within the range) are shown in Table 2. The groups are arranged in order of increasing momentum, L denoting a low field group and H a high field group. At the limiting momentum in each measurement there is an appreciable probability of contamination with particles of the opposite sign due to the finite resolution of the equipment. In order to avoid any uncertainty in the interpretation of the results, small deflexions in which the possibility of contamination is present are excluded from the analysis. Further, a small correction (less than 3 per cent. in the extreme case) is applied to the vertical measurements of the charge ratio to allow for the protons present in the penetrating component (Mylroi and Wilson 1951). No reliable data are available on this subject in the inclined directions but the subsequent error in the experimental charge ratios is expected to be less than 3 per cent.

The experimental values of the charge ratio are summarized in Table 2 and displayed in Figure 4. The results obtained in the vertical direction are shown together with the curve, representing the best estimate from available data, published by Owen and Wilson (1951). The measurements by these authors and by Beretta *et al.* (1953) possess considerably greater statistical accuracy than that attained in the present investigation ; however, it will be shown later that our results agree satisfactorily with the work of these authors.

The main feature of interest in the present investigation is the behaviour of the charge ratio at inclined directions in the east-west plane. Examination of Figure 4 shows that large deviations from the values recorded in the vertical direction occur at each zenith angle. Several features are immediately evident. In the western azimuth the charge ratio progressively increases with decreasing momentum, the magnitude of this increase being accentuated at the greater zenith angles. The reverse effect occurs at easterly zenith angles and for sufficiently low momenta a negative excess is obtained.

Evidence of this phenomena has been obtained by several other authors (Groetzinger and McClure 1950 ; Beretta, Filosofo, and Sommacal 1952 ; Quercia and Rispoli 1953), all using magnetic lens techniques to separate the particles. Beretta and his co-workers made measurements of the positive excess of mesons with energies in the range 0·7–1·5 BeV, in the vertical direction and at angles of 45° to the east and west. Their results show a positive excess of $0 \cdot 41 \pm 0 \cdot 025$ and $0 \pm 0 \cdot 023$ for the penetrating component in the western and eastern azimuths. These results correspond to charge ratios of $1 \cdot 52 \pm 0 \cdot 04$ and $1 \cdot 0 \pm 0 \cdot 03$ respectively. These authors explained their results in terms of the curvature

TABLE 2

CHARGE RATIO OF THE PENETRATING COMPONENT AS A FUNCTION OF MOMENTUM

Group	Momentum Range (BeV/c)	Mean Momentum (BeV/c)	Charge Ratio								
			0°	30°				60°			
				W^+/W^-	E^+/E^-	W^+/E^-	E^+/W^-	W^+/W^-	E^+/E^-	W^+/E^-	E^+/W^-
L1	0·24–1·0	0·6	1·14±0·07	1·61±0·25	0·93±0·15	1·19±0·14	1·25±0·15	1·90±0·23	0·60±0·11	1·37±0·19	0·83±0·15
L2	1·0 –2·1	1·6	1·20±0·07	1·40±0·20	1·39±0·22	1·43±0·15	1·35±0·16	1·65±0·18	0·97±0·13	1·08±0·12	1·50±0·19
H3	1·3 –2·0	1·7	1·16±0·10	1·44±0·23	1·14±0·13	1·27±0·12	1·30±0·13	2·20±0·35	0·78±0·13	1·26±0·18	1·36±0·24
H4	2·0 –3·2	2·6	1·39±0·12	1·39±0·20	1·09±0·12	1·30±0·11	1·18±0·11	1·70±0·23	0·80±0·11	1·07±0·13	1·27±0·19
L5	2·1 –4·9	3·4	1·28±0·08	1·25±0·17	1·27±0·19	1·23±0·13	1·30±0·13	1·51±0·12	1·12±0·12	1·34±0·12	1·25±0·12
H6	3·2 –5·5	4·3	1·36±0·12	1·19±0·18	1·18±0·13	1·24±0·11	1·14±0·11	1·34±0·15	0·83±0·10	1·14±0·13	0·99±0·13
H7	5·5–35	9·0	1·38±0·12	1·50±0·21	1·40±0·13	1·31±0·11	1·59±0·14	1·29±0·10	1·23±0·10	1·17±0·10	1·34±0·11
Mean ..	.. ..	.. ..	1·266 ±0·035	1·385 ±0·054	1·202 ±0·039	1·279 ±0·045	1·300 ±0·048	1·537 ±0·061	0·979 ±0·044	1·208 ±0·049	1·244 ±0·056

of the meson trajectories in the magnetic field of the Earth and concluded that the charge ratio at production is the same at these angles as in the vertical direction. The more recent experiments of Quercia and Rispoli (1953) were performed at a number of zenith angles, and their results show the general effect. Following the method of analysis proposed by Beretta, Filosofo, and Sommacal (1952), these authors could not explain the large residual fluctuations of the charge ratios and no definite conclusions could be reached.

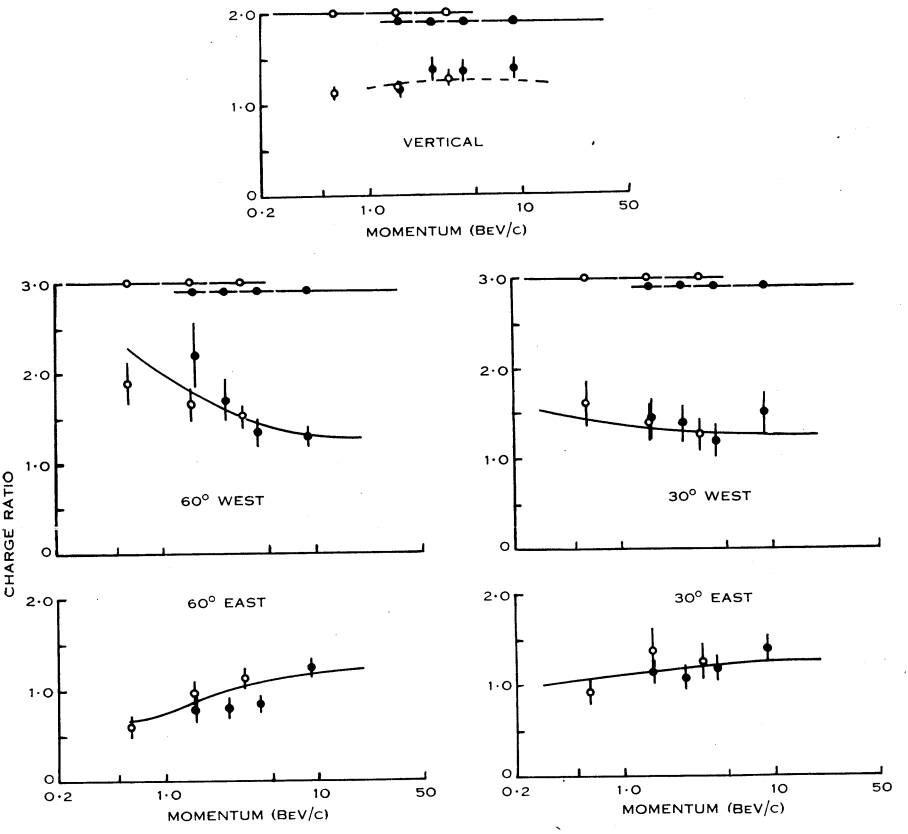

Fig. 4.—Charge ratio as a function of momentum.
○ 1900 G. ● 13,500 G.
----- From Owen and Wilson (1951).
——— Calculated.

Since the experiment was performed at a geomagnetic latitude of 47 °S, it is extremely unlikely that an asymmetry in the primary radiation large enough to explain this effect could exist. However, due to the Earth's magnetic field, positive and negative mesons recorded with sea-level momentum p_0 at a zenith angle θ in the east-west plane will have trajectories of the form shown in Figure 5. It is assumed that, on the average, the primary component traverses the same atmospheric thickness (g cm^{-2}) in each case before producing mesons. Denoting by x_0 the distance measured along the trajectory from the point of

observation to the production level, the charge ratio of the mesons at sea-level may be written as

$$\frac{w(x_0^+,p_0,\theta)}{w(x_0^-,p_0,\theta)} \cdot \frac{K^+p(x_0^+)^{-3}}{K^-p(x_0^-)^{-3}}=F(p_0,\,\theta,\,x_0^+,\,x_0^-)\frac{K^+}{K^-},$$

where $w(x_0, p_0, \theta)$ is the survival probability of mesons recorded at sea-level with momentum p_0 at the angle θ, $p(x_0)$ is the momentum at production, and $K^+(p)^{-3}$ and $K^-(p)^{-3}$ are the production spectra of the positive and negative mesons respectively. It is known from the vertical measurements that the charge ratio at production, K^+/K^-, is a slowly varying function of momentum. For the purpose of this discussion it may be considered constant.

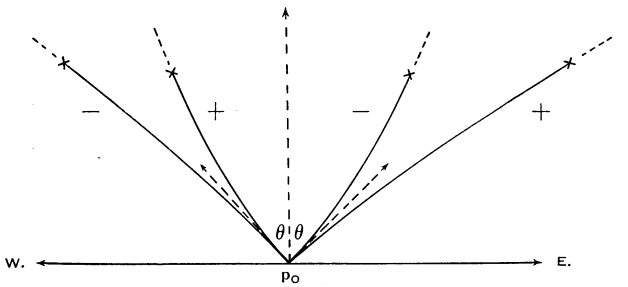

Fig. 5.—Meson trajectories in the Earth's magnetic field.

Reference to Figure 5 shows that in the eastern azimuth $x_0^+ > x_0^-$. Consequently

$$p(x_0^+) > p(x_0^-)$$

and

$$w(x_0^+,\,p_0,\,\theta) < w(x_0^-,\,p_0,\,\theta).$$

Therefore $F<1$ and decreases as $x_0^+ - x_0^-$ increases.

Since the radius of curvature of the trajectory at any point is inversely proportional to the momentum at that point, it follows that F decreases as p_0 is decreased or θ increased. Similar considerations apply in the western azimuth. Here $x_0^+ < x_0^-$ so that $F>1$ and increases as p_0 is decreased or θ increased.

The preceding discussion explains qualitatively the behaviour of the charge ratio in inclined directions. The vertical measurements are unaffected by the curvature since the trajectories of the positive and negative mesons are symmetrical about the zenith giving $x_0^+ = x_0^-$ and hence $F=1$. It was pointed out by Beretta, Filosofo, and Sommacal (1952) that, in fact, all the meson trajectories are symmetrical about the zenith. Thus, for the charge ratios W^+/E^- and and E^+/W^- the factor $F=1$ under all circumstances and the observed values of these ratios at sea-level give a measure of the mean charge ratio at production.

The ratios W^+/E^- and E^+/W^- are collected in Table 2. The mean values shown represent suitably weighted averages over the spectrum. It is seen that those for W^+/E^- and E^+/W^- do not differ significantly from the mean $1\cdot266 \pm 0\cdot035$ recorded in the vertical direction. Examination of the individual

points indicates that, although large fluctuations about the mean value occur, there is no systematic variation with either zenith angle or momentum. A χ^2 test has been performed to ascertain whether these deviations were consistent with that expected from random fluctuation of the points. The following measurements have been tested against the curve published by Owen and Wilson (1951): the vertical ratios, the 30° W^+/E^- and E^+/W^-, the 60° W^+/E^- and E^+/W^-. The confidence levels obtained were 70, 90, 20, 50, and 8 per cent. respectively. All of these lie within the normal limits 5–95 per cent. Corresponding tests on the 30° W^+/W^- and E^+/E^-, and the 60° W^+/W^- and E^+/E^- gave the values 2, 2, 0·01, and 0·01 per cent., thus verifying the systematic deviation illustrated in Figure 4.

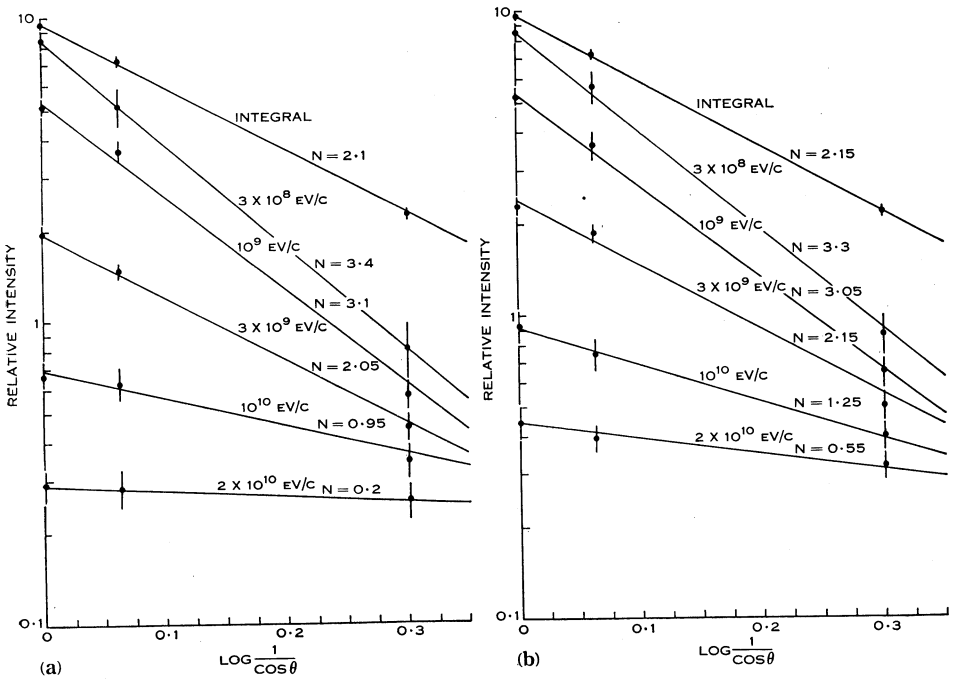

Fig. 6.—Variation of intensity I_θ with zenith angle θ at particular momenta, (*a*) to the east; (*b*) to the west.

$$I_\theta = I_0 \cos^n \theta.$$

As a final test, an approximate calculation of the charge ratios W^+/W^- and E^+/E^- was made by the method outlined earlier in the discussion. An approximate numerical evaluation of the path lengths x_0^+ and x_0^- allowed values of the factor F to be calculated. Assuming a value 1·25 for the charge ratio at production the curves shown in Figure 4 with the 30° and 60° measurements were obtained. The reasonable agreement with this approximate calculation, together with the previous tests, allows the conclusion that the behaviour of the charge ratio at inclined directions is explained as a secondary effect due to curvature of the meson trajectories in the magnetic field of the Earth.

(c) *The Intensity as a Function of Zenith Angle*

Previous work on this subject (Greisen 1942 ; Kraushaar 1949 ; Zar 1951 ; and others) has shown that in most instances the results could be fitted satisfactorily by a law of the form

$$I_\theta = I_0 \cos^n \theta,$$

where I_θ is the intensity at a zenith angle θ. A value of $n=2\cdot1$ for the total penetrating component was obtained by Greisen (1942). However, delayed coincidence and anti-coincidence experiments on low momentum mesons (Kraushaar 1949 ; Zar 1951) have shown that the value of n may be as high as $3\cdot3$ in this region. No comprehensive measurements on the behaviour of n as a function of momentum are available. Although the statistical accuracy of the present measurements is not sufficient to provide a rigorous test of this expression, by assuming its validity the behaviour of the exponent n with momentum may be obtained.

The intensity of the total penetrating component and the differential intensity at five values of the momentum are plotted against θ in Figure 6. Figure 6 (*a*) refers to measurements made in the eastern azimuth and Figure 6 (*b*) to the corresponding measurements in the western azimuth. Values of $n=2\cdot1$ and $2\cdot15$ are obtained for the total penetrating component, in good agreement with previous investigations. However, for mesons of $0\cdot3$ BeV/c the values $n=3\cdot3$ and $3\cdot4$ are recorded (compare Kraushaar (1949) and Zar (1951)) and as the momentum increases the value of n decreases until the sea-level radiation at these latitudes becomes substantially isotropic above 20 BeV/c.

V. Acknowledgments

The authors wish to thank Professor L. H. Martin for his interest in this work. They are indebted to Dr. H. D. Rathgeber, who suggested the investigation, for helpful discussions and advice on technical aspects throughout the project. The assistance of Mr. J. L. Rouse in the early part of the experiment is greatly appreciated.

VI. References

Beretta, E., Filosofo, I., and Sommacal, B. (1952).—*Nuovo Cim.* **9** : 317.
Beretta, E., Filosofo, I., Sommacal, B., and Puppi, G. (1953).—*Nuovo Cim.* **10** : 1354.
Brown, R. H., et al. (1949).—*Phil. Mag.* **40** : 862.
Burbury, D. W. P., and Fenton, K. B. (1952).—*Aust. J. Sci. Res.* A **5** : 47.
Caro, D. E., Parry, J. K., and Rathgeber, H. D. (1951).—*Aust. J. Sci. Res.* A **4** : 16.
Euler, H., and Heisenberg, W. (1938).—*Ergebn. exakt. Naturw.* **17** : 1.
Fenton, K. B. (1952).—Ph.D. Thesis, University of Tasmania.
Greisen, K. (1942).—*Phys. Rev.* **61** : 212.
Groetzinger, G., and McClure, G. W. (1950).—*Phys. Rev.* **77** : 777.
Janossy, J., and Wilson, J. G. (1946).—*Nature* **158** : 450.
Kraushaar, W. L. (1949).—*Phys. Rev.* **76** : 1045.
Mylroi, M. G., and Wilson, J. G. (1951).—*Proc. Phys. Soc. Lond.* A **64** : 404.
Owen, B. G., and Wilson, J. G. (1951).—*Proc. Phys. Soc. Lond.* A **64** : 417.
Quercia, I. F., and Rispoli, B. (1953).—*Nuovo Cim.* **10** : 357.
Sands, M. (1950).—*Phys. Rev.* **77** : 180.
Wilson, J. G. (1946).—*Nature* **158** : 414.
Zar, J. L. (1951).—*Phys. Rev.* **83** : 761.